How to cite: *Angew. Chem. Int. Ed.* **2024**, *63*, e202411438
doi.org/10.1002/anie.202411438

Photopharmacology Hot Paper

Photo-BQCA: Positive Allosteric Modulators Enabling Optical Control of the M_1 Receptor

*Hubert Gerwe[+], Eva Schaller[+], Rosalba Sortino, Ekin Opar, Joaquín Martínez-Tambella, Marcel Bermudez, J. Robert Lane, Pau Gorostiza, and Michael Decker**

Abstract: The field of G protein-coupled receptor (GPCR) research has greatly benefited from the spatiotemporal resolution provided by light controllable, *i.e.*, photoswitchable ligands. Most of the developed tools have targeted the Rhodopsin-like family (Class A), the largest family of GPCRs. However, to date, all such Class A photoswitchable ligands were designed to act at the orthosteric binding site of these receptors. Herein, we report the development of the first photoswitchable allosteric modulators of Class A GPCRs, designed to target the M_1 muscarinic acetylcholine receptor. The presented benzyl quinolone carboxylic acid (BQCA) derivatives, Photo-BQC*is*A and Photo-BQC*tr*A*ns*, exhibit complementary photopharmacological behavior and allow reversible control of the receptor using light as an external stimulus. This makes them valuable tools to further investigate M_1 receptor signaling and a proof of concept for photoswitchable allosteric modulators at Class A receptors.

Introduction

G protein-coupled receptors (GPCRs) are of exceptional therapeutic value, being directly or indirectly targeted by approximately one third of FDA-approved drugs.[1] However, some GPCR subfamilies have proven challenging to address in drug discovery, as selectivity among their subtypes is very difficult to achieve. The five muscarinic acetylcholine receptor (mAChR or simply MR) subtypes are prototypically difficult to target with selectivity. This is essentially caused by the high degree of homology within the orthosteric binding sites of these receptor subtypes. In contrast to the orthosteric binding site, topographically distinct allosteric binding sites are often less conserved, thus enabling the development of subtype-selective ligands with a diverse range of functions.[2–3] The development of photoswitchable ligands, *i.e.*, molecules that reversibly change their chemical structure and concomitantly their biological activity upon illumination, has provided pharmacological and biomedical research with the ability to turn a given receptor into an artificial photoreceptor. A plethora of light controllable GPCR ligands was developed which found application in a variety of pharmacological settings.[4–19] Amongst the different GPCR classes, the Rhodopsin-like family (Class A) has so far received the highest interest.[20–24] For a more detailed picture about the successes and limitations of photoswitchable GPCR ligands, the reader can consult previous reviews about that topic.[4–5,20] Many prior studies focused on photoswitchable MR ligands yielding efficacy-switchable ligands, bistable, visible light photoswitchable M_1R agonists or M_2R agonists with in vivo applications.[25–28] Unfortunately, those ligands were either not subtype-selective or showed only slight selectivity over other receptor subtypes.[25–28] Although developing photoswitchable ligands targeting allosteric binding sites is a

[*] H. Gerwe,[+] E. Schaller,[+] Prof. Dr. M. Decker
Pharmaceutical and Medicinal Chemistry
Institute of Pharmacy and Food Chemistry, Julius Maximilian University of Würzburg (JMU)
Am Hubland, 97074 Würzburg (Germany)
E-mail: michael.decker@uni-wuerzburg.de

R. Sortino, E. Opar, J. Martínez-Tambella, Prof. Dr. P. Gorostiza
Institute for Bioengineering of Catalonia (IBEC), The Barcelona Institute of Science and Technology
Carrer de Baldiri Reixac, 10–12, 08028 Barcelona (Spain)

R. Sortino, E. Opar, J. Martínez-Tambella, Prof. Dr. P. Gorostiza
CIBER-BBN, ISCIII
Carrer de Melchor Fernández Almagro, 3, 28029 Madrid (Spain)

R. Sortino, E. Opar, J. Martínez-Tambella
University of Barcelona—Doctoral program, Barcelona, 08007 Spain

Prof. Dr. M. Bermudez
Institute of Pharmaceutical and Medicinal Chemistry, University of Münster
Corrensstr. 48, 48149 Münster (Germany)

Dr. J. R. Lane
(1) Centre of Membrane Proteins and Receptors (COMPARE) and (2) Dept. of Physiology, Pharmacology and Neuroscience, School of Life Sciences, Queen's Medical Centre University of Nottingham Nottingham, NG7 2UH, UK

Prof. Dr. P. Gorostiza
Catalan Institution of Research and Advanced Studies (ICREA)
Passeig de Lluís Companys, 23, 08010 Barcelona (Spain)

[+] These authors contributed equally to this work.

promising approach to overcome selectivity issues, so far, no such ligand has been published for Class A GPCRs. However, other GPCR classes have been successfully addressed with photoswitchable allosteric modulators, demonstrating the value of combining subtype selectivity achieved by allosteric ligands with the precision of photoswitchable compounds.[29–35] Applying this promising approach to Class A GPCRs, we selected a subfamily prototypical for allosteric modulation: mAChR.[36] Since all the closely related mAChRs (M_1-M_5) subtypes are therapeutically important targets, various subtype selective positive allosteric modulators (PAMs) have been developed.[36–37] For this study, the first PAM reported for the muscarinic receptors, benzyl quinolone carboxylic acid (BQCA), was especially appealing since comprehensive structure–activity relationships (SARs) are available.[38–41]

Here, we present the first two reversibly photoswitchable allosteric modulators for Class A GPCRs. Based on BQCA, an iterative approach was used to find and enhance functional photoswitching at the M_1R. This resulted in a *cis*-on PAM we termed "Photo-BQC*is*A". In addition, a derivative with complementary photopharmacological properties (*trans*-on) termed "Photo-BQC*tr*A*ns*" was also synthesized and pharmacologically characterized.

Results and Discussion

The design of the presented photoswitchable allosteric modulators was based on SARs available for a variety of BQCA derivatives.[40–44] In general, SARs of BQCA can be classified in three categories (Figure 1): top-moiety, quinolone-core and non-planar arm. While the acid function of the top-moiety is not essential for allosteric affinity, it is essential for binding cooperativity. If cooperativity is to be maintained, its substitution is only possible in exchange with a hydrogen bond donor in the correct orientation.[40] However, the absence of the hydrogen bond donor does not impair affinity, which had allowed us in a preceding project to design the photoswitchable subtype selective dualsteric ligand BQCAAI.[25] Substitution at the quinolone-core modulates the intrinsic efficacy of the allosteric ligands, a property which is considered disadvantageous.[45–47] Moreover, none of the conducted SAR studies indicated that an "azo-substituent" at the core could be tolerated. In contrast to the former two positions, the non-planar arm has been shown to tolerate a huge variety of modifications and extensions with little impact on activity, hence its SARs are often described as "flat".[41,48] We reasoned that these "flat-SARs" would prevent any change of the pharmacological properties induced upon isomerization of a non-planar photoswitchable arm. Consequently, this part of BQCA seems rather ill suited for the introduction of the photoswitchable moiety. However, we deemed this an ideal starting point. Since introduction of an azobenzene moiety in this part doesn't lead to a loss of cooperativity but also doesn't show a difference between the photoisomers yet, it opens up the possibility to choose which isomer is more active by analyzing the effects of different substitution patterns on the distal benzene ring and exploiting them to yield the desired effect.

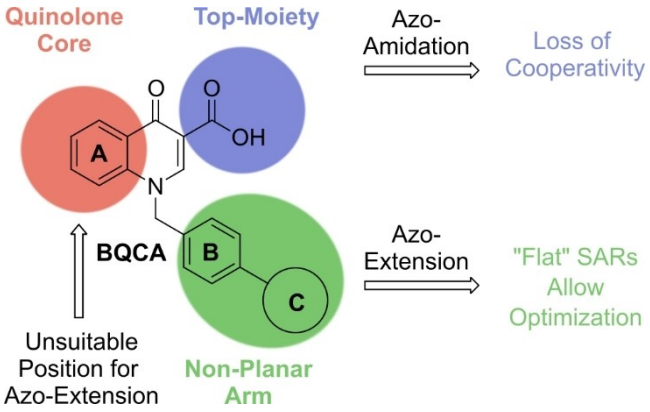

Figure 1. Structure–activity relationships of BQCA. While introduction of an azobenzene at the quinolone core and the top-group is predicted to be disadvantageous for cooperativity, modifications of the non-planar arm are plentiful and allow introduction of further ring systems without affecting the essential function of the compound.

Initially, two photoswitchable derivatives of 8-fluoro-BQCA (8F-BQCA) were synthesized to explore and validate the SAR landscape with photoswitchable moieties (Figure 2).[40] 8F was kept in this 1st generation to make the data as comparable as possible to BQCA itself. Starting with an "azo-amidation" of the carboxylic acid (**1**) and an "azo-extension" of the non-planar arm (**2**), the reported SARs were validated, and the focus shifted to the development of BQCAs bearing photoswitchable non-planar arms with different substitution patterns (Figure 2). 8F substitution was omitted in the 2nd generation as it is reported to only increase the intrinsic agonist efficacy without increasing the desired cooperativity.

Among the vast amount of non-planar arm modifications with little impact on activity, an interesting behavior towards C-ring methylation patterns can be found in the literature. Depending on the position on the C-ring, methyl groups either have no impact or are detrimental for the compound's potency.[41] Considered irrelevant for optimizing BQCA itself, it provided us with a vulnerability that a photoswitch might exploit. To examine whether C-ring methylation might be used as an impairing motive which could be switched in and out of the "weak spot", a "methyl walk" on the distal azobenzene ring was realized synthetically (**3**–**5**; Figure 2). Simultaneously, we also explored whether the quinolone core could be attached in *meta* position (*meta*-linked) with respect to the azo moiety (**6**). Based on the results (see below) a 3rd series of Photo-BQCAs was obtained exploiting the *ortho* position of the distal benzene ring (**7a**–**g**; Figure 2). Simultaneously, to demonstrate that the flat-SAR approach can be utilized to develop complementary photopharmacological behavior, a *trans*-on Photo-BQCA (**8**) was developed. This development was based on the assumption that a pyrazole-based photoswitch forms a more T-shaped *cis*-isomer compared to an azobenzene[49] making the *cis*-isomer too bulky to fit into the binding

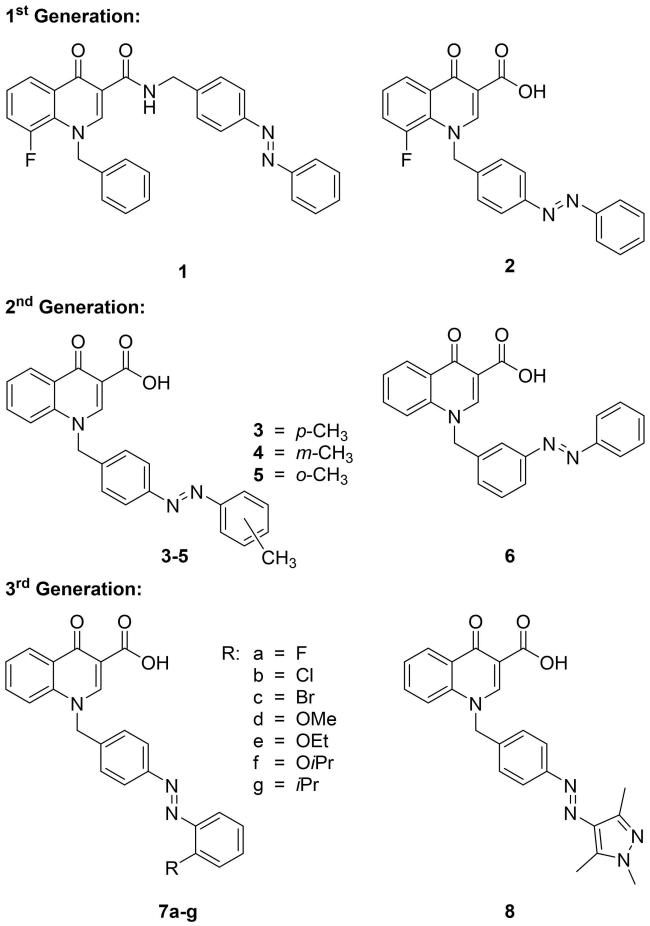

Figure 2. Overview over photoswitchable BQCA derivatives designed for optical control of M_1R activation.

pocket. With the pyrazole-switch, the *trans*-isomer on the other hand is small enough to fit into the allosteric pocket unlike the *ortho*-substituted azobenzenes. The synthesis of the 3rd generation of Photo-BQCAs is described in the following (Scheme 1), for synthetic schemes and details concerning Photo-BQCAs **1**–**6** see Supporting Information (Scheme S1–S3).

The quinolone-core (**10**) was synthesized as reported.[40] Instead of the typically employed, low yielding and laborious thermal cyclization of (phenylamino)methylene malonates in phenylether at over 200 °C,[25,50] an improved cyclization using Eaton's Reagent was employed to give compound **10** in good yields.[51–52] Subsequent *N*-benzylation with 1-(bromomethyl)-4-nitrobenzene followed by reduction of the *para*-nitro compound **11** yielded the corresponding aniline **12**. Aniline **12** was partially oxidized to the nitroso compound **13** using Oxone® in a heterogeneous H_2O/CH_2Cl_2 system. This gave access to derivatization by condensation of compound **13** with various commercially available anilines in a Baeyer-Mills reaction to the corresponding azobenzenes (**14a**–**g**). Finally, the desired free carboxylic acids (**7a**–**g**) were obtained under basic hydrolysis of the ester moiety. The *trans*-on heteroarene photoswitchable ligand[53] (**8**) was synthesized from aniline **12** which was converted into the corresponding diazonium salt and used in situ to form a phenylhydrazono moiety (**15**) by reaction with pentane-2,4-dione. Subsequent cyclization with mono-methyl hydrazine yielded the desired pyrazole/benzene photoswitch (**16**) which had to be hydrolyzed as described above to obtain the target carboxylic acid (**8**).

Determination of photophysical properties of all synthesized ligands by UV/Vis spectroscopy revealed that all compounds can be maximally photo-isomerized to the *cis*-configuration using light of 365 nm. Notably, all *ortho*-alkoxy substituted Photo-BQCAs (**7d**–**f**) and the pyrazole/benzene photoswitchable ligand **8** can also be effectively *cis*-enriched using a higher wavelength of 385 nm. *Trans*-enrichment of all azobenzene based Photo-BQCAs was achieved using 400 or 455 nm, while the pyrazole/benzene photoswitchable ligand **8** was maximally *trans*-isomerized using green or orange light (530/590 nm). However, irradiation with orange light needs a prolonged duration of irradiation (10 min), hence 530 nm was used in all experiments. Concerning other relevant photophysical properties (ratios of photostationary states, resistance to photofatigue and thermal stability), all Photo-BQCAs behaved as expected (see Supporting Information for photophysical details).

All potential photoswitchable PAMs were evaluated in vitro at their maximally *cis*/*trans*-enriched photostationary states (in the following termed simply *cis*/*trans*-state) to test their ability to increase the potency of the orthosteric muscarinic agonist carbachol (CCh) at the human M_1R (hM_1R). For this purpose, a concentration-response of CCh was measured alone and in the presence of 1 μM pre-illuminated Photo-BQCAs in either *cis*- or *trans*-state. The respective wavelengths are noted in Figure 3. Human embryonic kidney (HEK) 293T cells expressing the hM_1R and a split luciferase-based probe for quantitative proximal determination of $G_{\alpha q}$ signaling in live cells were used. The probe detects interactions between $G_{\alpha q}$ and its effector phospholipase C-β3 (PLC-β3) as a quantifiable parameter of receptor activation.[54] The wavelengths applied in this assay do not influence the compounds' photoisomerization (bio-orthogonal assay).[25–26]

As expected, the amide **1** showed no cooperativity with CCh in either of its photoforms while the unsubstituted, *para*-linked photoswitchable non-planar arm (**2**) exhibited BQCA-like (EC_{50}(CCh + BQCA) = 55 nM) cooperativity which was independent of the photoswitch configuration (EC_{50}(CCh + *cis*-**2**) = 47 nM; EC_{50}(CCh + *trans*-**2**) = 52 nM; Figure 1A, Figure S18). Evaluation of the 2nd generation of Photo-BQCAs (**3**–**6**), Figure 1B, Figure S19) showed that in fact positioning of the methyl-group could heavily influence the pharmacological properties of the allosteric ligands. While the *para*-methyl compound (**3**) was devoid of any cooperativity in both photoforms and behaved like compound **1**, the *meta*-methyl substituted Photo-BQCA (**4**) showed some, however, reduced cooperativity with no *cis*/*trans* differences (EC_{50}(CCh + *cis*-**4**) = 91 nM; EC_{50}(CCh + *trans*-**4**) = 93 nM). Strikingly, the *ortho*-methyl compound (**5**) exhibited BQCA-like cooperativity and additionally minor differences between the activity of the photoforms favoring the *cis*-isomer (EC_{50}(CCh + *cis*-**5**) = 47 nM;

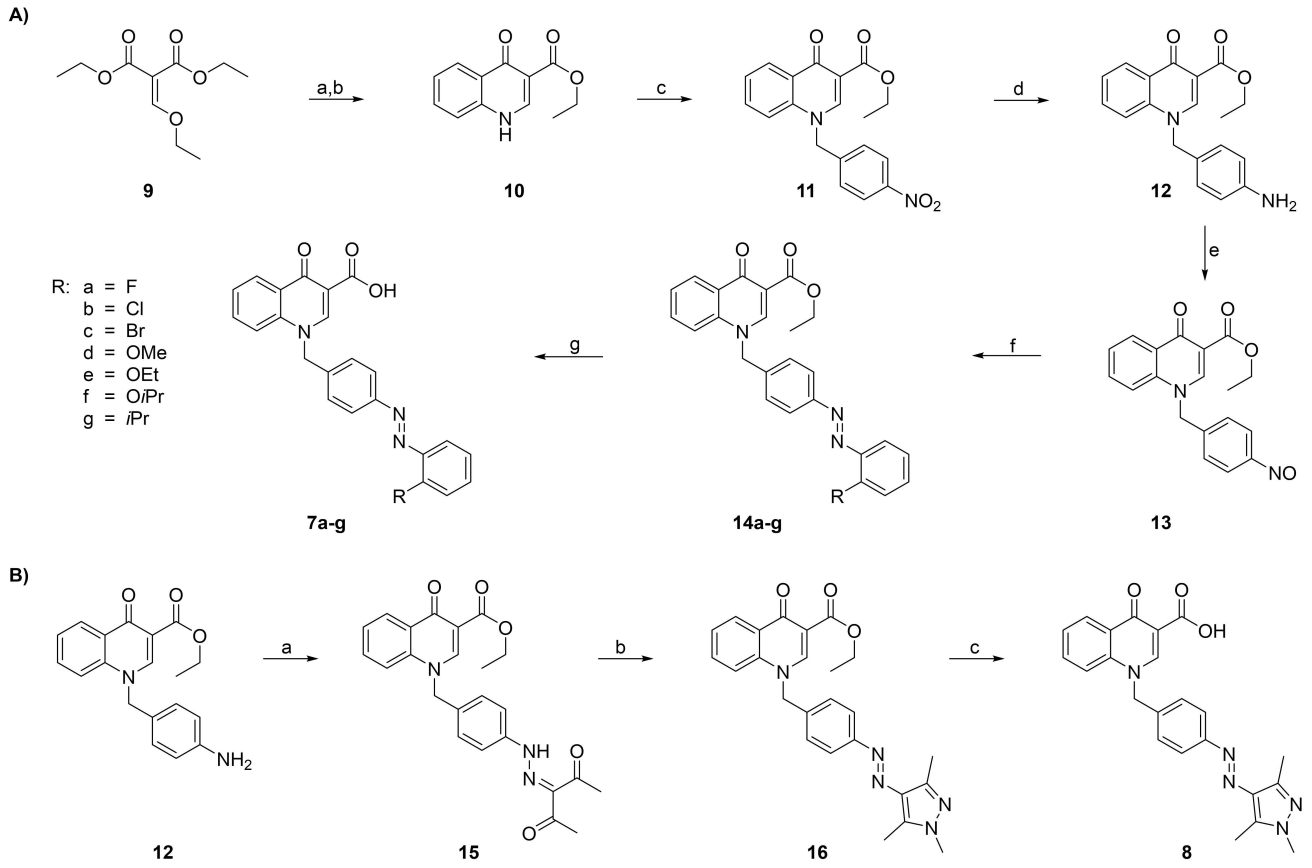

Scheme 1. (A) Synthetic route to benzyl azo-quinoline-carboxylic-acid derivatives of the 3rd generation. Reagents and conditions: a) aniline, 130 °C, 86 %; b) Eaton's reagent (Phosphorus pentoxide, 7.7 wt % in methanesulfonic acid), 130 °C, 77 %; c) 1-(bromomethyl)-4-nitrobenzene, K_2CO_3, KI, DMF, RT, 89 %; d) Fe, NH_4Cl, H_2O, EtOH, 80 °C, quant. e) Oxone®, CH_2Cl_2, H_2O, RT, 83 %; f) respective aniline, HOAc, RT, 53–92 %; g) 1 N NaOH, THF, 50 °C, 59–92 %. (B) Synthetic route to the 1,3,5-trimethyl-pyrazole photoswitch. Reagents and conditions: a) 1. $NaNO_2$, H_2O, AcOH, HCl, 0 °C; 2. pentane-2,4-dione, NaOAc, EtOH, H_2O, 0 °C→RT, 60 %; b) mono-methyl hydrazine, ethanol, 80 °C, 71 %; c) 1 N NaOH, THF, 50 °C, 79 %.

EC_{50}(CCh + *trans*-**5**) = 75 nM; Figure 1 B). Interestingly, *meta*-linked compound **6** also showed significant cooperation and a minor *cis*-on difference, however, the latter was considerably lower than that of compound **5** (see Figure S19), thus we focused on the *ortho* position.

The results are in accordance with the prediction that the essential parameter to induce *cis*/*trans* activity differences is the size of the *ortho*-substituent at the distal benzene ring. This trend was observed for electron withdrawing substituents (F < Cl < Br) as well as for electron donating substituents (MeO < EtO < *i*PrO). The latter showed increased cooperativity in comparison to BQCA (see Table S1 for comprehensive overview). However, as optimization of the allosteric modulating capability was not within the scope of this work, we did not further investigate which of the cooperativity parameters was increased.

The greatest separation between the *cis*-state and *trans*-state concentration-response curves was achieved using the *ortho*-isopropyl compound (Photo-BQC*is*A, **7g**; (EC_{50}(CCh + *cis*-**7g**) = 55 nM; EC_{50}(CCh + *trans*-**7g**) = 152 nM)) and the 1,3,5-trimethyl-pyrazole photoswitch (Photo-BQC*tr*A*ns*, **8**; (EC_{50}(CCh + *cis*-**8**) = 156 nM; EC_{50}(CCh + *trans*-**8**) = 56 nM)). Both showed an approximately 3fold increase upon irradiation with the respective wavelength. According to the molecular docking (see below), the *cis*/*trans* activity difference is in each case induced by steric hindrance unilaterally affecting one of the two isomers. This is also reflected by the *in vitro* results, as both active isomers are identical to BQCA regarding their overall cooperativity, while the inactive configuration is almost identical to the CCh curve. While ligand **7g** is more active in its UV light (365 nm) induced, thermodynamically less stable *cis*-configuration, compound **8** is more active in the thermodynamically more stable *trans*-configuration which can be enriched using green light (530 nm). In total, both ligands show complementary photopharmacological behavior. We then tested for the combined allosteric parameters by measuring concentration-response curves of CCh with different modulator concentrations (Supplementary Figure S21 and Table S2) and fitting the curves with an operational model of allosterism and agonism.[55] Nonetheless, the fitted values do not represent affinity and/or cooperativity values of the isolated isoforms because at either light wavelength condition both photoisomers are present to a different extent. Furthermore, to prove subtype selectivity, we tested **7g** and **8** for allosteric modulation at the closely related subtypes M_3 and M_5

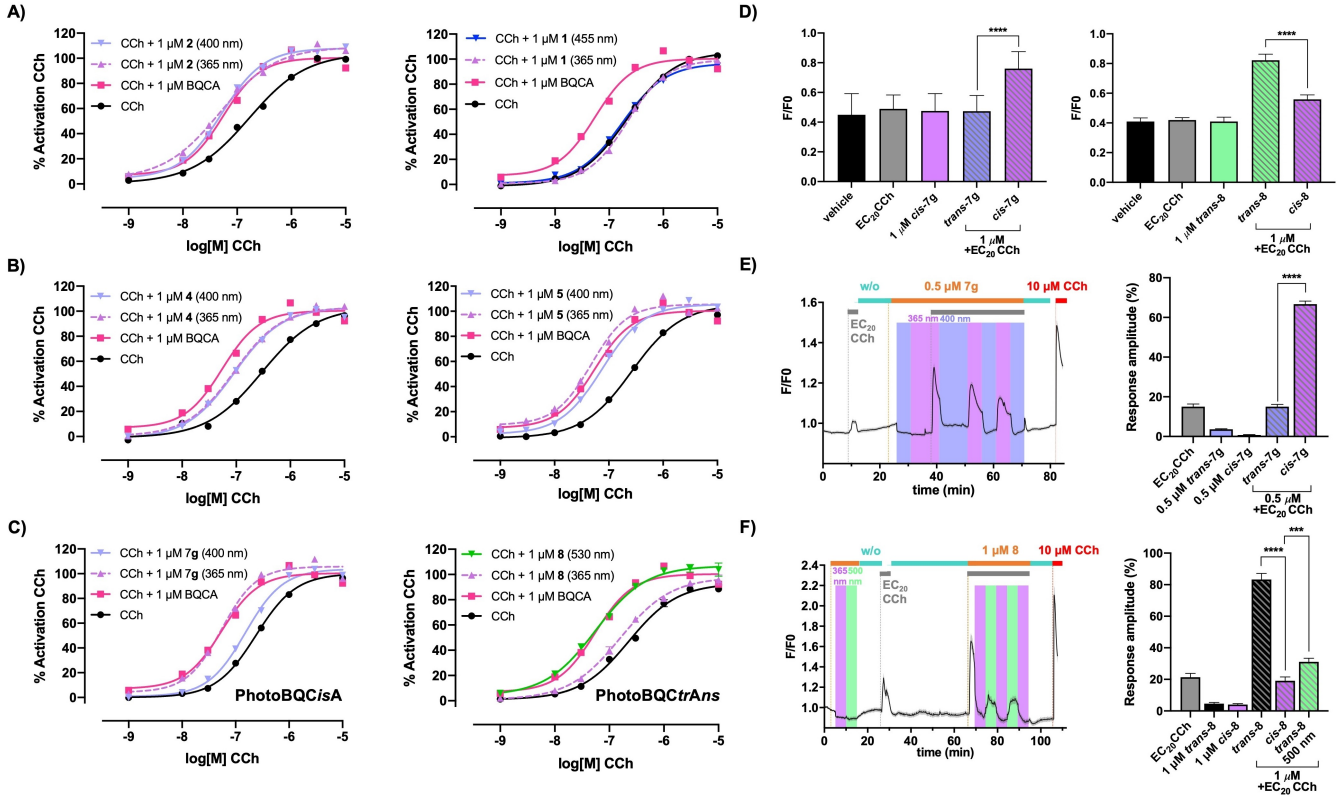

Figure 3. (A–C) In vitro characterization of potential photo-PAMs using a split luciferase complementation-based protein-protein interaction assay detecting the interaction between $G_{\alpha q}$ and its effector phospholipase C-β3 (PLC-β3) as a quantifiable parameter of receptor activation.[54] Concentration-response curves of muscarinic orthosteric agonist carbachol (CCh) alone and in presence of 1 μM pre-illuminated Photo-BQCAs in either *cis*- and *trans*-state. BQCA (1 μM) was included as reference. Data are given as the mean ± standard error of mean (SEM) of 3 independent experiments performed in duplicate and normalized over the maximum response of CCh. (D) In vitro characterization of ligands **7g** and **8** using a plate reader-based fluorescence assay. The functional activity of the hM$_1$Rs was measured by the increase of intracellular Ca^{2+} in HEK tsA201 cells co-expressing the receptor and the Ca^{2+} indicator GCaMP6s (n = 5 independent experiments). Only the application of the *cis*-**7g** or *trans*-**8** together with CCh at its EC_{20} elicited significant response (irradiation: *cis*-**7g**, *cis*-**8**: 365 nm; *trans*-**7g**: 400 nm; *trans*-**8**: 530 nm). The amplitude of the response was quantified and compared by the one-way ANOVA with Tukey's multiple comparisons post-hoc test c[**7g**], c[**8**] = 1 μM (****$p < 0.0001$ for vehicle *vs* active isomer + EC_{20} CCh; ****$p < 0.0001$ for EC_{20} CCh *vs* active isomer + EC_{20} CCh; ****$p < 0.0001$ for active isomer *vs* active isomer + EC_{20} CCh; ****$p < 0.0001$ for inactive isomer + EC_{20} CCh *vs* active isomer + EC_{20} CCh) Data were normalized over the maximum response obtained with the saturation concentration of CCh (30 μM) and all statistical analyses were performed with GraphPad Prism 9. Error bars are ± SEM. (E,F) In vitro characterization of ligands **7g** (E) and **8** (F) using a live Ca^{2+} imaging assay. Real time Ca^{2+} imaging response (averaged traces on the left, black line, $n = 116$ cells, E; $n = 47$ cells, F) in HEK tsA201 cells co-expressing hM$_1$R and GCaMP6s. Colored bars (grey, orange and red) indicate application of the respective cpd. in the given concentration or washout phases (turquoise). Colored rectangles show periods of illumination (violet = 365 nm, blue 400 nm, green = 500 nm). Shadow represents ± SEM. The quantification was made by calculating the amplitude of the response (right panel, $n = 221$ cells E; $n = 86$ cells F). The amplitude of the response (%) reached by the application of *cis*-**7g** + EC_{20} CCh and *trans*-**7g** + EC_{20} CCh was 66.6 ± 1.5 and 15 ± 1.5, respectively. In addition, for the *trans*-**8** + EC_{20} CCh and *cis*-**8** + EC_{20} CCh, it was 83.3 ± 3.7 and 19.1 ± 2.3, respectively. Data were normalized over the maximum response obtained with the saturation concentration of CCh (10 μM) and were analyzed using GraphPad Prism 9 by paired-sample Wilcoxon signed-rank test. (c[**7g**] = 0.5 μM, c[**8**] = 1 μM; ****$p < 0.0001$ for EC_{20} CCh *vs* active isomer; ****$p < 0.0001$ for EC_{20} CCh *vs* inactive isomer; n.s. for EC_{20} CCh *vs* inactive isomer + EC_{20} CCh; ****$p < 0.0001$ for EC_{20} CCh *vs* *cis*-**7g** + EC_{20} CCh; ****$p < 0.0001$ for EC_{20} CCh *vs* *trans*-**8** EC_{20} CCh; **$p < 0.01$ for EC_{20} CCh *vs* *trans*-**8** 500 nm; ****$p < 0.0001$ for inactive isomer *vs* inactive isomer + EC_{20} CCh; ****$p < 0.0001$ for active isomer *vs* inactive isomer + EC_{20} CCh; ****$p < 0.0001$ for active isomer *vs* active isomer + EC_{20} CCh; ****$p < 0.0001$ for inactive isomer *vs* active isomer + EC_{20} CCh; ****$p < 0.0001$ for *cis*-**7g** + EC_{20} CCh *vs* *trans*-**7g** + EC_{20} CCh; ; ****$p < 0.0001$ for *cis*-**8** + EC_{20} CCh *vs* *trans*-**8** + EC_{20} CCh; ***$p < 0.001$ for *cis*-**8** + EC_{20} CCh *vs* *trans*-**8** 500 nm + EC_{20} CCh; ****$p < 0.0001$ for *trans*-**8** + EC_{20} CCh *vs* *trans*-**8** 500 nm + EC_{20} CCh.

resulting in no positive allosteric modulation (Supplementary Figure S22).

Next, to validate our results, we evaluated the receptor functional activation through a plate reader-based fluorescence assay by measuring increases in intracellular calcium. This assay was performed in HEK tsA201 cells co-expressing the hM$_1$R and GCaMP6s (excitation 488 nm, emission 510 nm) as a genetically encoded calcium sensor. The intracellular calcium release and fluorescence increase upon receptor activation occurs only when the ligands **7g** or **8** are applied in their active configurations together with CCh as prestimulant (EC_{20}) (Figure 3D). To ensure complete photoconversion to the *cis* active form before adding CCh, a longer lag time was applied during the first

irradiation with 365 nm for compound **7g**. These results confirm that both compounds act as PAMs of M_1R, with the ligand **7g** being more active in its *cis*- and **8** in its *trans*-photoform, respectively. In agreement with previous results, no agonistic effect was observed, and no receptor response was caused by the vehicle. CCh at saturation concentrations was used as a positive control and to normalize the data. No calcium responses were observed in HEK cells not expressing M_1R (Figure S23A,B). Moreover, we were interested to evaluate Photo-BQC*is*A and Photo-BQC*tr*A*ns* in a downstream calcium imaging assay for their ability to allow reversible modulation of receptor signaling (Figure 3E,F). Fluorescence imaging was performed with the calcium sensor GCaMP6s using CCh as prestimulant (EC_{20}) and positive control (10 μM). First, the intrinsic agonist activity of both compounds was assessed before and after isomerization into the active photoform and no increase in intracellular calcium was observed. Subsequently, cytosolic calcium oscillations on prestimulated cells were induced by addition of *cis*-enriched Photo-BQC*is*A. Photoconversion of Photo-BQC*is*A into its *trans*-photoform resulted in a sharp decline of fluorescence response which could be switched on and off reversibly (Figure 3 E and S24A). The same dynamic photomodulation of receptor activity was possible using Photo-BQC*tr*A*ns* (Figure 3F and S24B). However, smaller calcium responses were elicited for the latter when exposed to 500 nm illumination, indicating that this wavelength might not be the optimal choice for *cis*-to-*trans* isomerization of this compound. For this reason, for Photo-BQC*tr*A*ns* the experiments were also conducted using a red-shifted calcium sensor, R-GECO1, with excitation at 562 nm and emission at 600 nm.[56] This was done to maintain consistency with the *cis*-to-*trans* isomerization wavelength used in previous assays (530 nm) (Figure S25 and S24 C). Despite the lower responses (probably due to the sensor's lower calcium sensitivity) the effect of Photo-BQC*tr*A*ns* is in agreement with previous results. The responses under the application of the compounds and upon photoconversion with given wavelengths for the selected compounds were quantified by peak amplitude and the analysis showed an almost complete on/off switching (Figure 3 E, F and S25). However, for compound **8** the *cis*-to-*trans* isomerization under illumination with 500 nm reached the 30 % of the response observed for the compound applied in dark. Fluorescence photoresponses were only observed in cells expressing M_1Rs (Supplementary Figure S23C,D).

Having proven the efficacy and photomodulation of compounds in two different in vitro assays, we decided to assess the potential applicability of compound **7g** in vivo, with endogenous M_1Rs, ACh concentrations, and dynamics, respectively. We used a locomotion assay on 7 days post-fertilization blinded zebrafish larvae (*Danio rerio*).[19] This model presents several advantages, such as their transparency (that allows regulation of drug activity upon light illumination with high spatial-temporal resolution), their genetic similarity to humans, and their rapid development, which permits the study of neural circuits, including muscarinic modulation in a short period of time. Moreover, it has been described that locomotion hyperactivity in zebrafish larvae caused by both acute and long-term exposure to the cholinergic agonist arecoline could be mediated by mAChRs. This behavior was attenuated by M_1 antagonist VU0255035, suggesting that M_1 activation could lead to increased motility in zebrafish larvae, while its blockade could result in diminished motility.[57] Zebrafish larvae can be acutely blinded by a short-term exposure to high intensity light (>120.000 lux), which can significantly reduce the impact of light on their locomotion (Figure S26).[19] Therefore, we assessed the effect of compound **7g** on the swimming distance of zebrafish larvae in darkness, under 365 nm, and under 400 nm illumination. Strikingly, larvae showed a 7-fold increase in locomotor activity compared to the vehicle during the UV periods when **7g** is isomerized to its *cis*-active photoform. Conversely, no differences were observed in darkness or under blue irradiation, where the less active *trans*-isomer is predominant (Figure 4).

Based on recent insights into the nature of the ("cryptic") allosteric binding pocket,[58] the behavior of the presented Photo-BQCAs can be structurally explained. Despite the flexible nature of this cryptic binding pocket, its size and the possibility to bind lipophilic building blocks are limited and therefore provide a rational way to design configuration-specific photoswitchable ligands (Figure 5, Supplementary Figure S27). While the cryptic binding pocket can host an azobenzene moiety in *cis*- and *trans*-configuration, size and substitution pattern of the photoswitchable scaffold account for the specificity of the allosteric effect by distinct configurations. A plausible bind-

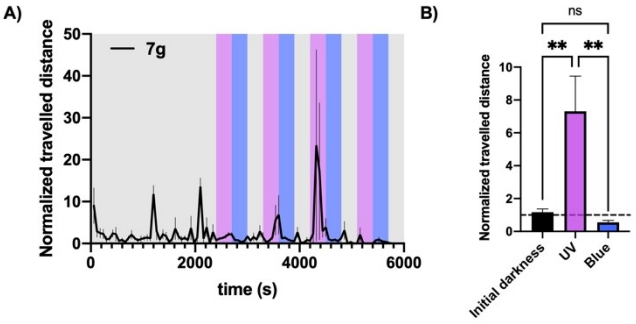

Figure 4. (A) Distance travelled by 7 days post-fertilization blinded zebrafish larvae preincubated for 80 min with compound **7g** (30 μM) throughout a 100 min protocol. Colored rectangles show periods of illumination (violet = 365 nm, blue 400 nm, grey = darkness). The trace corresponds to the average of $n = 12$ larvae trajectories ± standard error of mean (SEM) in one independent experiment. (B) Quantification of the distances swum by the treatment group (30 μM of compound **7g**) during the initial darkness period of the protocol (40 min) and last 2 cycles of UV-blue illumination having accomplished a preincubation with **7g** of 2 h 30 min ±10 min. The normalized travel distance for the different experimental conditions is 1.1 ± 0.2 for the initial darkness, 7.3 ± 2.1 under UV light; 0.5 ± 0.12 under illumination with blue light. Data were normalized to the distance travelled by blinded zebrafish larvae at same age incubated with vehicle (0.3 % DMSO, dotted-line), are shown as mean ± SEM from two independent experiments ($n = 12$ individuals/group/exp), and were analyzed by RM one-way ANOVA with Holm-Šídák's multiple comparisons test, **$p < 0.01$ initial darkness *vs* UV; **$p < 0.01$ UV *vs* blue; n.s. initial darkness *vs* blue.

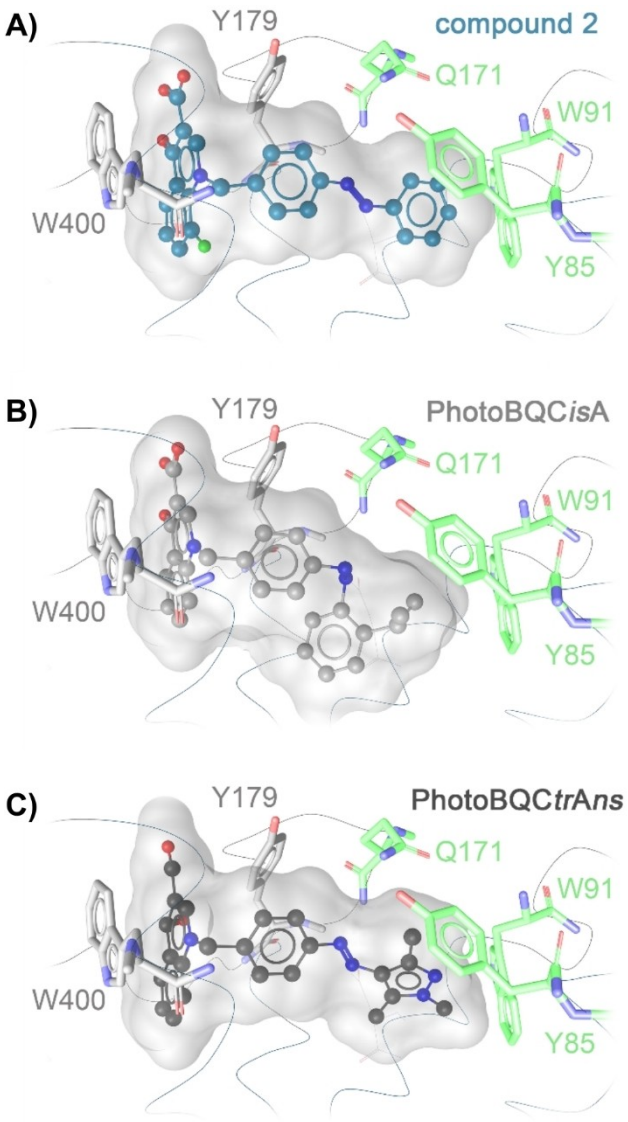

Figure 5. Proposed binding modes of compound **2** (A), PhotoBQC*is*A **7g** (B), and PhotoBQC*trAns* **8** (C) indicate a similar orientation in the extracellular receptor region. The quinolone core of all compounds is located between the allosteric key residues W400 and Y179 (light grey), and the photoswitchable building block is pointing in the previously reported cryptic binding pocket for which important residues are highlighted in green. Docking into the cryptic binding pocket was performed with Autodock 4.2 as implemented in LigandScout 4.4. with iterative side chain optimization to account for the flexibility of the cryptic binding pocket.

ing mode of PhotoBQC*is*A **7g** in its *trans* configuration could not be found without disturbing the placement of the quinolone moiety between W400 and Y179. Photo-BQC*tr*A*ns* **8** fits in the cryptic binding pocket in its *trans* configuration. The proposed binding orientation was also supported by all-atoms molecular dynamics simulations (Supplementary Figure S28). We surmise that the additional methyl groups might lead to a conformation of the *cis*-configuration that is less favorable for binding within the cryptic binding pocket.

Conclusion

The development of subtype selective allosteric ligands has been an important focus in the development of potential therapeutics, especially for the Class A GPCR subfamily of mAChRs. Many ligands have been designed successfully, exhibiting unprecedented selectivity at, for example, the M_1 subtype.[36] However, those ligands have failed as they still cause a variety of muscarinic adverse effects (, *i.e.*, seizures).[59] These are either caused by excessive activation of the receptor and/or due to activation of the receptor in tissues mediating an unwanted physiological effect.[59] A photopharmacological allosteric modulator would be inherently resistant towards this kind of issues, due to the possibility to precisely determine the location of action as well as its maximal activity. However, no such photoswitchable allosteric modulators have been reported for Class A GPCRs so far.

Here, we described the design, synthesis, and biological evaluation of the first reversibly photoswitchable allosteric modulators for Class A GPCRs, based on the prototypical M_1 PAM, namely BQCA. Notably, we proved our design hypothesis that introduction of the azobenzene in a position known to exhibit "flat-SARs" would enable deliberate development of both a *cis*-on and a *trans*-on Photo-BQCA. This approach was motivated by the goal of a more knowledge-based approach in finding a photoswitchable compound with desirable properties, as was also argued in a most recent review.[60] Hence, we focused on hypothesis-driven iterations of design-make-test-analyze (DMTA) cycles.[61–62]

The Photo-BQCAs developed in this study were termed according to their more active isomer, Photo-BQC*is*A and Photo-BQC*tr*A*ns*. At typical PAM concentrations, photo-BQC*is*A is inactive in the dark and can be activated using UV light (365 nm). At the same concentration, Photo-BQC*tr*A*ns* is active in the dark-adapted *trans*-state, which can also be enriched with green light (530 nm). This allows activation of the preirradiated *cis*-photoform with light of deeper tissue penetrating capabilities than 365 nm. At BQCA-like concentrations both compounds allow dynamic photopotentiation of calcium activity in vitro and of locomotion in vivo. As such, we think that Photo-BQC*is*A and Photo-BQC*tr*A*ns* will follow the example of Class B and C GPCR allosteric photoswitches, constituting interesting and useful tool compounds in the ongoing efforts to understand the complex signaling mechanism of GPCRs.

Author Contributions

H.G. and E.S. contributed equally to this work. R.S. and E.O. contributed equally to this work. All authors have given approval to the final version of the manuscript.

Acknowledgements

H.G. and M.D. acknowledge the support by the International Doctoral Program "Receptor Dynamics: Emerging Paradigms for Novel Drugs" funded within the framework of the Elite Network of Bavaria (ENB). Financial support by the German Research Foundation (DFG) under DE1546/12-1 is acknowledged. M.B. thanks the German Research Foundation DFG (Grant: 407626949). E.S. acknowledges a PhD scholarship by the German Academic Scholarship Foundation (Studienstiftung des deutschen Volkes) and support by the Marianne-Plehn-Program of the Elite Network of Bavaria (ENB). Moreover, IBEC acknowledges the support from the EU Horizon 2020 Framework Programme for Research and Innovation, including the European Innovation Council Pathfinder (Phototheraport, 101130883), Human Brain Project (WaveScalES, SGA3, 945539), and Information and Communication Technologies (Deeper, ICT-36-2020-101016787). It was also supported by the Government of Catalonia (CERCA Programme; AGAUR 2021-SGR-01410); by the Spanish Ministry of Science and Innovation (DEEP RED, grant PID2019-111493RB-I00; EPILLUM, grant AEI/10.13039/501100011033; and Research Network in Biomedicine eBrains-Spain, RED2022-134823-E). R. S. was supported by a predoctoral fellowship FPI (reference BES-2017-082496). We thank Sam Hollingsworth and Ron Dror for sharing atom coordinates of the M_1 cryptic binding pocket. TOC was created with BioRender.com. Open Access funding enabled and organized by Projekt DEAL.

Conflict of Interest

The authors declare no conflict of interest.

Data Availability Statement

The data that support the findings of this study are available in the supplementary material of this article.

Keywords: GPCR · photopharmacology · allosterism · muscarinic ligands · photoswitch

[1] A. S. Hauser, M. M. Attwood, M. Rask-Andersen, H. B. Schioth, D. E. Gloriam, *Nat. Rev. Drug Discov.* **2017**, *16*, 829–842.
[2] H. H. Nickols, P. J. Conn, *Neurobiol. Dis.* **2014**, *61*, 55–71.
[3] S. Granier, B. Kobilka, *Nat. Chem. Biol.* **2012**, *8*, 670–673.
[4] K. Hull, J. Morstein, D. Trauner, *Chem. Rev.* **2018**, *118*, 10710–10747.
[5] M. Ricart-Ortega, J. Font, A. Llebaria, *Mol. Cell. Endocrinol.* **2019**, *488*, 36–51.
[6] X. Gomez-Santacana, S. M. de Munnik, P. Vijayachandran, D. Da Costa Pereira, J. P. M. Bebelman, I. J. P. de Esch, H. F. Vischer, M. Wijtmans, R. Leurs, *Angew. Chem. Int. Ed.* **2018**, *57*, 11608–11612.
[7] K. Rustler, S. Pockes, B. König, *ChemMedChem* **2019**, *14*, 636–644.
[8] D. Lachmann, A. Konieczny, M. Keller, B. König, *Org. Biomol. Chem.* **2019**, *17*, 2467–2478.
[9] N. J. Hauwert, T. A. M. Mocking, D. Da Costa Pereira, K. Lion, Y. Huppelschoten, H. F. Vischer, I. J. P. De Esch, M. Wijtmans, R. Leurs, *Angew. Chem. Int. Ed.* **2019**, *58*, 4531–4535.
[10] A. Acosta-Ruiz, V. A. Gutzeit, M. J. Skelly, S. Meadows, J. Lee, P. Parekh, A. G. Orr, C. Liston, K. E. Pleil, J. Broichhagen, J. Levitz, *Neuron* **2020**, *105*, 446–463.e413.
[11] P. Donthamsetti, N. Winter, A. Hoagland, C. Stanley, M. Visel, S. Lammel, D. Trauner, E. Isacoff, *Nat. Commun.* **2021**, *12*, 4775.
[12] V. A. Gutzeit, A. Acosta-Ruiz, H. Munguba, S. Hafner, A. Landra-Willm, B. Mathes, J. Mony, D. Yarotski, K. Borjesson, C. Liston, G. Sandoz, J. Levitz, J. Broichhagen, *Cell Chem. Biol.* **2021**, *28*, 1648–1663.e1616.
[13] F. Riefolo, R. Sortino, C. Matera, E. Claro, B. Preda, S. Vitiello, S. Traserra, M. Jimenez, P. Gorostiza, *J. Med. Chem.* **2021**, *64*, 9259–9270.
[14] J. Morstein, G. Romano, B. E. Hetzler, A. Plante, C. Haake, J. Levitz, D. Trauner, *Angew. Chem. Int. Ed.* **2022**, *61*, e202117094.
[15] A. Garrido-Charles, A. Huet, C. Matera, A. Thirumalai, J. Hernando, A. Llebaria, T. Moser, P. Gorostiza, *J. Am. Chem. Soc.* **2022**, *144*, 9229–9239.
[16] H. Gerwe, F. He, E. Pottie, C. Stove, M. Decker, *Angew. Chem. Int. Ed.* **2022**, *61*, e202203034.
[17] R. Bosma, N. C. Dijon, Y. Zheng, H. Schihada, N. J. Hauwert, S. Shi, M. Arimont, R. Riemens, H. Custers, A. van de Stolpe, H. F. Vischer, M. Wijtmans, N. D. Holliday, D. W. D. Kuster, R. Leurs, *iScience* **2022**, *25*, 104882.
[18] R. Lahmy, H. Hubner, M. F. Schmidt, D. Lachmann, P. Gmeiner, B. König, *Chem. Eur. J.* **2022**, *28*, e202201515.
[19] C. Matera, P. Calve, V. Casado-Anguera, R. Sortino, A. M. J. Gomila, E. Moreno, T. Gener, C. Delgado-Sallent, P. Nebot, D. Costazza, S. Conde-Berriozabal, M. Masana, J. Hernando, V. Casado, M. V. Puig, P. Gorostiza, *Int. J. Mol. Sci.* **2022**, *23*.
[20] M. Wijtmans, I. Josimovic, H. F. Vischer, R. Leurs, *Curr. Opin. Pharmacol.* **2022**, *63*, 102192.
[21] M. V. Westphal, M. A. Schafroth, R. C. Sarott, M. A. Imhof, C. P. Bold, P. Leippe, A. Dhopeshwarkar, J. M. Grandner, V. Katritch, K. Mackie, D. Trauner, E. M. Carreira, J. A. Frank, *J. Am. Chem. Soc.* **2017**, *139*, 18206–18212.
[22] A. Duran-Corbera, J. Catena, M. Otero-Vinas, A. Llebaria, X. Rovira, *J. Med. Chem.* **2020**, *63*, 8458–8470.
[23] A. Sink, H. Gerwe, H. Hubner, V. Boivin-Jahns, J. Fender, K. Lorenz, P. Gmeiner, M. Decker, *Chem. Eur. J.* **2024**, *30*, e202303506.
[24] N. J. Hauwert, T. A. M. Mocking, D. Da Costa Pereira, A. J. Kooistra, L. M. Wijnen, G. C. M. Vreeker, E. W. E. Verweij, A. H. De Boer, M. J. Smit, C. De Graaf, H. F. Vischer, I. J. P. de Esch, M. Wijtmans, R. Leurs, *J. Am. Chem. Soc.* **2018**, *140*, 4232–4243.
[25] L. Agnetta, M. Kauk, M. C. A. Canizal, R. Messerer, U. Holzgrabe, C. Hoffmann, M. Decker, *Angew. Chem. Int. Ed.* **2017**, *56*, 7282–7287.
[26] L. Agnetta, M. Bermudez, F. Riefolo, C. Matera, E. Claro, R. Messerer, T. Littmann, G. Wolber, U. Holzgrabe, M. Decker, *J. Med. Chem.* **2019**, *62*, 3009–3020.
[27] F. Riefolo, C. Matera, A. Garrido-Charles, A. M. J. Gomila, R. Sortino, L. Agnetta, E. Claro, R. Masgrau, U. Holzgrabe, M. Batlle, M. Decker, E. Guasch, P. Gorostiza, *J. Am. Chem. Soc.* **2019**, *141*, 7628–7636.
[28] A. Barbero-Castillo, F. Riefolo, C. Matera, S. Caldas-Martinez, P. Mateos-Aparicio, J. F. Weinert, A. Garrido-Charles, E.

Claro, M. V. Sanchez-Vives, P. Gorostiza, *Adv. Sci.* **2021**, *8*, e2005027.
[29] S. Pittolo, X. Gomez-Santacana, K. Eckelt, X. Rovira, J. Dalton, C. Goudet, J. P. Pin, A. Llobet, J. Giraldo, A. Llebaria, P. Gorostiza, *Nat. Chem. Biol.* **2014**, *10*, 813–815.
[30] J. Broichhagen, N. R. Johnston, Y. von Ohlen, H. Meyer-Berg, B. J. Jones, S. R. Bloom, G. A. Rutter, D. Trauner, D. J. Hodson, *Angew. Chem. Int. Ed.* **2016**, *55*, 5865–5868.
[31] B. J. Jones, R. Scopelliti, A. Tomas, S. R. Bloom, D. J. Hodson, J. Broichhagen, *ChemistryOpen* **2017**, *6*, 501–505.
[32] P. Donthamsetti, D. B. Konrad, B. Hetzler, Z. Fu, D. Trauner, E. Y. Isacoff, *J. Am. Chem. Soc.* **2021**, *143*, 8951–8956.
[33] X. Gomez-Santacana, S. Panarello, X. Rovira, A. Llebaria, *Curr. Opin. Pharmacol.* **2022**, *66*, 102266.
[34] S. Bossi, R. Helleringer, M. Galante, E. Monlleo, A. Trapero, X. Rovira, H. Daniel, A. Llebaria, H. McLean, *Front. Cell. Neurosci.* **2018**, *12*, 449.
[35] M. Ricart-Ortega, A. E. Berizzi, V. Pereira, F. Malhaire, J. Catena, J. Font, X. Gomez-Santacana, L. Munoz, C. Zussy, C. Serra, X. Rovira, C. Goudet, A. Llebaria, *ACS Pharmacol. Transl. Sci.* **2020**, *3*, 883–895.
[36] J. Jakubik, E. E. El-Fakahany, *Biomol. Eng.* **2020**, *10*.
[37] A. Bock, R. Schrage, K. Mohr, *Neuropharmacology* **2018**, *136*, 427–437.
[38] L. Ma, M. A. Seager, M. Wittmann, M. Jacobson, D. Bickel, M. Burno, K. Jones, V. K. Graufelds, G. Xu, M. Pearson, A. McCampbell, R. Gaspar, P. Shughrue, A. Danziger, C. Regan, R. Flick, D. Pascarella, S. Garson, S. Doran, C. Kreatsoulas, L. Veng, C. W. Lindsley, W. Shipe, S. Kuduk, C. Sur, G. Kinney, G. R. Seabrook, W. J. Ray, *Proc. Natl. Acad. Sci. USA* **2009**, *106*, 15950–15955.
[39] J. K. Shirey, A. E. Brady, P. J. Jones, A. A. Davis, T. M. Bridges, J. P. Kennedy, S. B. Jadhav, U. N. Menon, Z. Xiang, M. L. Watson, E. P. Christian, J. J. Doherty, M. C. Quirk, D. H. Snyder, J. J. Lah, A. I. Levey, M. M. Nicolle, C. W. Lindsley, P. J. Conn, *J. Neurosci.* **2009**, *29*, 14271–14286.
[40] S. N. Mistry, C. Valant, P. M. Sexton, B. Capuano, A. Christopoulos, P. J. Scammells, *J. Med. Chem.* **2013**, *56*, 5151–5172.
[41] S. D. Kuduk, D. C. Beshore, *Curr. Top. Med. Chem.* **2014**, *14*, 1738–1754.
[42] J. C. C. Dallagnol, E. Khajehali, E. T. van der Westhuizen, M. Jorg, C. Valant, A. G. Goncalves, B. Capuano, A. Christopoulos, P. J. Scammells, *J. Med. Chem.* **2018**, *61*, 2875–2894.
[43] M. Jorg, E. T. van der Westhuizen, E. Khajehali, W. A. C. Burger, J. M. White, K. H. C. Choy, A. B. Tobin, P. M. Sexton, C. Valant, B. Capuano, A. Christopoulos, P. J. Scammells, *ACS Chem. Neurosci.* **2019**, *10*, 1099–1114.
[44] M. Jorg, E. Khajehali, E. T. van der Westhuizen, C. C. KH, D. M. Shackleford, A. B. Tobin, P. M. Sexton, C. Valant, B. Capuano, A. Christopoulos, P. J. Scammells, *ChemMedChem* **2021**, *16*, 216–233.
[45] J. W. Cruickshank, S. M. Brudzynski, R. S. McLachlan, *Brain Res.* **1994**, *643*, 125–129.
[46] A. Alt, A. Pendri, R. L. Bertekap Jr., G. Li, Y. Benitex, M. Nophsker, K. L. Rockwell, N. T. Burford, C. S. Sum, J. Chen, J. J. Herbst, M. Ferrante, A. Hendricson, M. E. Cvijic, R. S. Westphal, J. O'Connell, M. Banks, L. Zhang, R. G. Gentles, S. Jenkins, J. Loy, J. E. Macor, *J. Pharmacol. Exp. Ther.* **2016**, *356*, 293–304.
[47] J. M. Rook, M. Abe, H. P. Cho, K. D. Nance, V. B. Luscombe, J. J. Adams, J. W. Dickerson, D. H. Remke, P. M. Garcia-Barrantes, D. W. Engers, J. L. Engers, S. Chang, J. J. Foster, A. L. Blobaum, C. M. Niswender, C. K. Jones, P. J. Conn, C. W. Lindsley, *ACS Chem. Neurosci.* **2017**, *8*, 866–883.
[48] S. Johnstone, J. S. Albert, *Bioorg. Med. Chem. Lett.* **2017**, *27*, 2239–2258.
[49] J. Calbo, C. E. Weston, A. J. White, H. S. Rzepa, J. Contreras-Garcia, M. J. Fuchter, *J. Am. Chem. Soc.* **2017**, *139*, 1261–1274.
[50] S. Schramm, L. Agnetta, M. Bermudez, H. Gerwe, M. Irmen, J. Holze, T. Littmann, G. Wolber, C. Trankle, M. Decker, *ChemMedChem* **2019**, *14*, 1349–1358.
[51] P. E. Eaton, G. R. Carlson, J. T. Lee, *J. Org. Chem.* **2002**, *38*, 4071–4073.
[52] D. Zewge, C. Y. Chen, C. Deer, P. G. Dormer, D. L. Hughes, *J. Org. Chem.* **2007**, *72*, 4276–4279.
[53] C. E. Weston, R. D. Richardson, P. R. Haycock, A. J. White, M. J. Fuchter, *J. Am. Chem. Soc.* **2014**, *136*, 11878–11881.
[54] T. Littmann, T. Ozawa, C. Hoffmann, A. Buschauer, G. Bernhardt, *Sci. Rep.* **2018**, *8*, 17179.
[55] K. Leach, R. E. Loiacono, C. C. Felder, D. L. McKinzie, A. Mogg, D. B. Shaw, P. M. Sexton, A. Christopoulos, *Neuropsychopharmacol.* **2010**, *35*, 855–869.
[56] D. S. Kim, V. Jayaraman, L. L. Looger, K. Svoboda, *Soc. Neurosci.* **2014**, 11–19.
[57] P. Siregar, G. Audira, L. Y. Feng, J. H. Lee, F. Santoso, W. H. Yu, Y. H. Lai, J. H. Li, Y. T. Lin, J. R. Chen, C. D. Hsiao, *Toxin Rev.* **2021**, *13*.
[58] S. A. Hollingsworth, B. Kelly, C. Valant, J. A. Michaelis, O. Mastromihalis, G. Thompson, A. J. Venkatakrishnan, S. Hertig, P. J. Scammells, P. M. Sexton, C. C. Felder, A. Christopoulos, R. O. Dror, *Nat. Commun.* **2019**, *10*, 3289.
[59] H. T. M. Nguyen, E. T. van der Westhuizen, C. J. Langmead, A. B. Tobin, P. M. Sexton, A. Christopoulos, C. Valant, *Br. J. Pharmacol.* **2022**.
[60] P. Kobauri, F. J. Dekker, W. Szymanski, B. L. Feringa, *Angew. Chem. Int. Ed.* **2023**, *62*, e202300681.
[61] K. Hinnah, S. Willems, J. Morstein, J. Heering, F. W. W. Hartrampf, J. Broichhagen, P. Leippe, D. Merk, D. Trauner, *J. Med. Chem.* **2020**, *63*, 10908–10920.
[62] P. Kobauri, N. S. Galenkamp, A. M. Schulte, J. de Vries, N. A. Simeth, G. Maglia, S. Thallmair, D. Kolarski, W. Szymanski, B. L. Feringa, *J. Med. Chem.* **2022**, *65*, 4798–4817.

Manuscript received: June 18, 2024
Accepted manuscript online: August 13, 2024
Version of record online: October 8, 2024